THE JOURNAL OF PHYSICAL CHEMISTRY C

Article

pubs.acs.org/JPCC

Inducing Porosity on Hollow Nanoparticles by Hypervelocity Impacts

Felipe J. Valencia,[†,‡,¶] Rafael I. González,[†,‡,§] J. A. Valdivia,[†,‡] Miguel Kiwi,[*,†,‡] Eduardo M. Bringa,[∥] and José Rogan[†,‡]

[†]Departamento de Física, Facultad de Ciencias, Universidad de Chile, Casilla 653, Santiago, Chile 7800024

[‡]Centro para el Desarrollo de la Nanociencia y la Nanotecnología, CEDENNA, Avda. Ecuador 3493, Santiago, Chile 9170124

[¶]Núcleo de Matemáticas, Física y Estadítica, Facultad de Ciencias, Universidad Mayor, Manuel Montt 367, Providencia, Santiago, Chile

[§]Centro de Genómica y Bioinformática, Facultad de Ciencias, Universidad Mayor, Santiago, Chile

[∥]CONICET and Facultad de Ciencias Exactas y Naturales, Universidad Nacional de Cuyo, Mendoza 5500, Argentina

ABSTRACT: The large surface-to-volume ratio of hollow palladium nanoparticles (hNPs) offers room to improve their hydrogen storage capacity as well as their catalytic activity. However, a less explored possibility is to use, in addition, the internal cavity. Here we explore, through classical molecular dynamics, the possibility of boring channels across the hNP wall by collision with solid Pd nanoprojectiles at high velocities, as well as their resilience to maintain their spherical geometry. We choose a stable hNP with an inner diameter of 13 nm and an outer diameter of 15 nm. The projectiles are Pd NPs of 1.5, 2.4, and 3.0 nm, respectively. We consider collision speeds between 3 and 15 km/s, with an impact parameter between 0 to 7 nm. Four different regimes, as a function of kinetic energy and impact parameter of the projectile, are found. For low speeds, the projectile is not able to penetrate the target and only creates surface craters. For a narrow range of intermediate speeds, the projectile enters the target, but the hNP shell is able to self-heal, either totally or partially. For large speeds, the projectile penetrates the target without altering its spherical hollow geometry, but for even larger speeds, the hNP collapses into a solid structure. The specific threshold speed for each regime depends on the mass and speed of the projectile. In all noncollapsing cases, the results show a linear relationship between projectile kinetic energy and crater or perforation size. We also studied its behavior when the hNP suffers successive collisions, finding that it keeps its hollow shape but forms faceted structures, such as nanoframes or hollow cuboctahedron nanoparticles. All of our results suggest that Pd hNPs, with adequate combinations of external radius and thickness are very robust, can withstand hypervelocity impacts and that channels can be opened to allow molecules to reach the internal cavity.

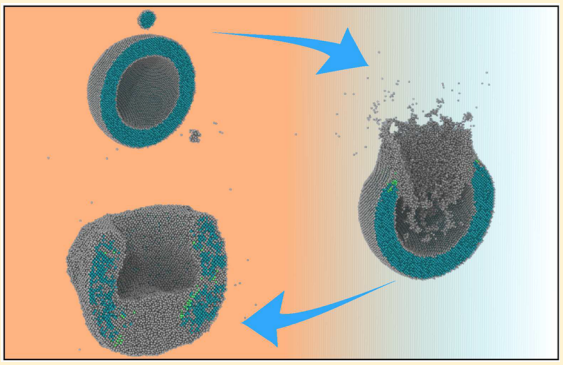

INTRODUCTION

Palladium has attracted significant interest for a long time due to its potential for hydrogen storage and its use in industrial catalysis processes.[1−3] In particular, hollow Pd nanoparticles (hNP), which have the advantage of low density and a large surface to volume ratio, have allowed for a significant efficiency increase of Pd nanostructures used in these endeavors.[4−7] These features have in turn motivated interesting experiments to synthesize Pd hNP of various shapes and sizes.[4,8−12] They range from a few nanometers to microns, depending on the synthesis protocol that is implemented.

In previous work, we found that the storage capacity efficiency enhancement relies mainly on the existence of the hNP cavity and the consequent large specific area.[13] However, most of the action takes place on the outer hNP surface due to the large energy cost for a molecule to cross from the outer hNP surface to the cavity, which reduces the usefulness of the presence of an internal surface. Therefore, gaining easy access to the interior cavity is the key to increase the efficient usage of hNPs. Progress has been achieved along these lines, like the inclusion of nanoporous shells[14−17] or dendritic-like hollow nanoparticles.[18] In both cases, the access to the cavity is due to the synthesis process, but it is of no use for an already synthesized hNP. A way to overcome this limitation is to open a hole or channel so that molecules can access the hNP interior. Precisely this subject is the main concern of this paper.

A natural way to achieve this goal is to bombard the hNP with a projectile of the proper size and speed to open such a channel. In fact, materials made of macroscopic hollow spheres are sometimes used to protect against hypervelocity impacts, due their ability to efficiently dissipate energy.[19,20] An important question, which we try to answer here, is if under this bombardment process the stability of the hNP is preserved. Notice that the energy of the projectile has to be large enough

Received: April 2, 2017
Revised: July 25, 2017
Published: July 25, 2017

DOI: 10.1021/acs.jpcc.7b03126
J. Phys. Chem. C 2017, 121, 17856−17861

for the channel to open, but the collision cannot be too violent to endanger structural stability.

hNPs are usually perceived as fragile structures, which subject to a perturbation will collapse into a solid and irregular NP. In fact, Jiang et al.[21] showed, by means of model calculations, that given certain relations between diameter and thickness, hNPs can collapse due to cavity-related stress. Moreover, this dynamic is enhanced by other factors like temperature and pressure.[22] In addition, a shrinkage of the hNP structure at temperatures below the melting point has been observed, leading to cavity collapse into a solid NP.[23−25] All these facts seem to provide arguments that point toward the unlikelihood that it is possible to modify hNP by means of collisions. However, we show below that there are scenarios in which the goal to bore channels in a Pd hNP is feasible.

In fact, our interest to explore the possibilities of boring channels to efficiently load the Pd hNP cavity is based on known results obtained for the mechanical properties of highly porous materials, as well as the scarcity of theoretical results on hNP subject to extreme conditions.[26,27] To pursue our objective, we simulate, by means of classical molecular dynamics (MD), the collision of hypervelocity nanoprojectiles (between 3 a 15 km/s) and Pd hNPs. In order to describe a variety of scenarios, different impact parameters are used, which allow one to generate a diversity of surface defects due to the large pressures and temperatures that develop as the projectile shares part of its energy with the hNP.

METHOD

Molecular dynamics is implemented by means of LAMMPS.[28] The Pd interatomic interaction potential we adopted is the Embedded Atom Method,[29] with the parameters by Sheng.[30] This way, properties like the melting point, liquid phase,[31] bulk modulus, and the electronic density of states for pressures up to 100 GPa[32] are properly described. This is an important issue when simulating ballistic problems because of the large pressures and temperatures that develop.

On the basis of the hNP stability criteria developed by Jiang et al.[21] and used by us[13] for Pd hNPs, we adopted as target a Pd hNP with an outer diameter of $40a_0$ (15 nm) and a wall thickness of $5a_0$ (2 nm), where a_0 = 0.389 nm is the Pd lattice parameter. As projectiles, Pd NPs 1.5, 2.4, and 3 nm in diameter, which correspond to 87, 144, 450, and 1061 atoms, respectively, were used. To ensure stability, and since the initial configuration is generally far from equilibrium, the hNP were relaxed at 300 K using the NVT ensemble with the Nosé−Hoover thermostat, during 400 ps, following previous work on Au and Pt[33] and Pd.[21,25] The hNP temperature was calculated as the average kinetic energy of the atoms, subtracting the velocity of the hNP center of mass. Moreover, the atoms ejected as a product of the collision are ignored when carrying out the statistics. The collision was simulated in the NVE ensemble and to ensure energy conservation at high velocities an adaptive time step, with a minimum value of 0.1 fs was adopted. After the collision, the system evolution is followed during 0.5 ns to make sure that the structure has not collapsed. Due to the relatively small energies involved, the electronic stopping power corresponds to only a small fraction,[34] which we neglect. The impact parameter was varied between 0 (head on collision) to $17.5a_0$. In order to obtain sufficient statistics, as well as representative results, each collision was repeated 20 times, varying the initial velocity distribution of projectile and target. The defect analysis was carried out using the common neighbor analysis (CNA), as implemented in OVITO.[35]

RESULTS

We start observing what happens to the hNP after it collides with a Pd_{140} projectile with a 10 km/s velocity. Our main concern is the stability of the hNP; and, if it collapses, to determine if it is due to the impact or to self-diffusion of the energy that the hNP does absorb in the process. In Figure 1a,

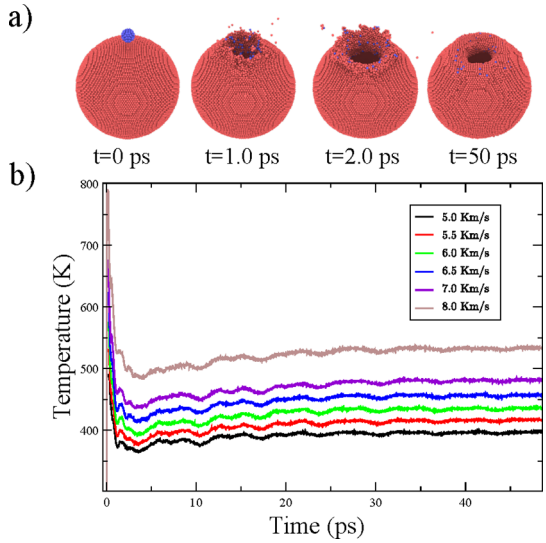

Figure 1. (a) Illustration after the collision between the Pd_{140}(blue) nanocluster and a Pd hNP (red). (b) Temperature of the hNP as a function of time.

we illustrate the temporal evolution and notice that, during the first picoseconds, the hNP shell is irreversibly perforated by the impact. Also during the first ∼2 ps, a temperature spike develops, shown in Figure 1b, which quite rapidly reaches a final equilibrium temperature determined by the projectile velocity. Since initially the hNPs are far from equilibrium, there is no well-defined criteria to establish when these structures are stable after the collision takes place. Furthermore, it is natural to observe the temperature increase on the basis of the projectile velocity. Hence, for small solid NPs, a critical point is to be expected near the NP melting point, which can be modeled by the $T = T_m(1 - c/r)$ law;[36] where T_m correspond to the material melting point, r is NP radius, and c a constant that depends on material properties, such as density, surface energy, etc. However, for hNPs, a first collapse occurs at temperatures below the NP melting point.[21,25] To the best of our knowledge, the only criterion to characterize the stability of hNP was proposed by Jiang et al.,[21] following either the energy or temperature fluctuations after long MD simulations. Since they are performed in the microcanical ensemble, an indication of the hNP stability can be obtained by monitoring changes in temperature, or abrupt kinetic energy fluctuations, during the simulation. By this reason, it is apparent that the temperature varies only slightly after 40 ps, followed for 500 ps to ensure that the hNP structure remains stable and that the temperature does not vary.

The size dependence of the projectile is shown in Figure 2. The Pd target was impacted with Pd NPs of 87, 144, and 450 atoms. Figure 2a illustrates the temperature dependence, Figure 2b the diameter of the channel that is created, and, Figure 2c

DOI: 10.1021/acs.jpcc.7b03126
J. Phys. Chem. C 2017, 121, 17856−17861

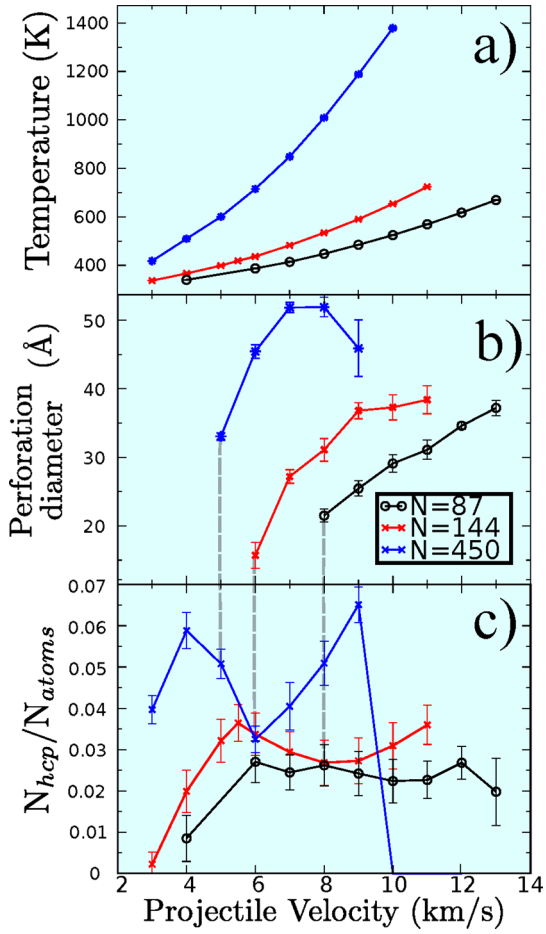

Figure 2. (a) Temperature, (b) perforation size, and (c) fraction of hcp as a function of projectile speed, for Pd projectiles of 87, 144, and 450 atoms. The gray dashed lines indicate the onset of shell perforation.

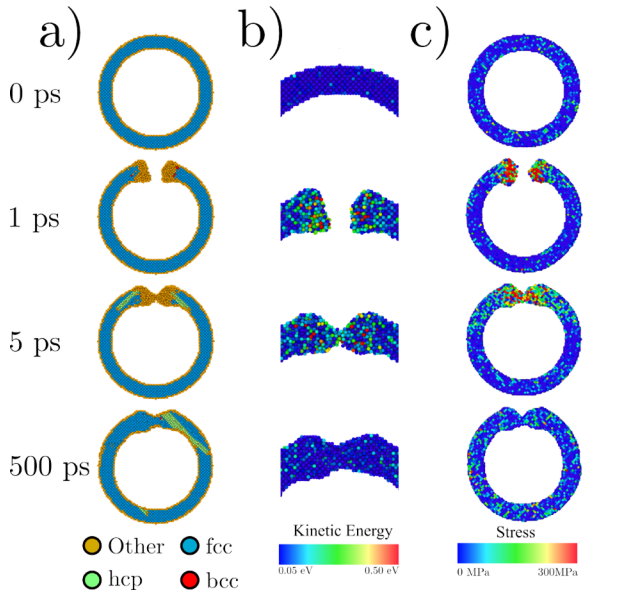

Figure 3. Cross section of the Pd hNP. (a) CNA analysis for different times after the collision. (b) Zoom of the perforation, where the color coding represents the kinetic energy of every atom. (c) Stress distribution.

the conversion to hcp crystal structure that ensues, all as a function of the projectile velocity. The temperature increase is proportional to the square of the velocity and to the mass of the projectile (i.e., as expected, it is proportional to its kinetic energy). Figure 2b shows that Pd_{87} and Pd_{144} projectiles are not large enough to induce instabilities in the hNP; however, Pd_{450} projectile impact raises the temperature above 1400 K and leads to the collapse of the hNP into a solid NP. Consequently, it is the melting of the hNP that sets an upper limit to the projectile mass. Actually, in Figure 2b, the gray dashed lines indicate the minimum projectile velocity required to obtain a permanent perforation of the hNP. The penetration velocity for hollow clusters is significantly larger than the predictions from an often used continuum model.[37] In fact, there are many differences between continuum and discrete penetration model results, as discussed by Higginbotham et al.[38] The diameter of the channel that opens increases with projectile size; however, as the temperature increases this diameter saturates, the structure shrinks as the hNP cools off, and the hNPs lose their spherical shape.

As far as the resulting hNP structure is concerned, Figure 2c shows that all the collisions imply a plastic target deformation,[39,40] where planar defects and twins are generated. While in solid NPs, no planar defects develop under similar conditions; in hNPs due to their geometry (that is, the presence of the cavity), the generation of defects is favored by the large stress on both the interior and exterior surfaces. In fact, three regimes are apparent: (i) for low projectile velocities there is a linear increase, as a function of velocity, of the defect creation; (ii) when the projectile is capable of perforating the hNP shell, the defect creation is reduced; and (iii) an increment of hcp is observed before the hNP collapses into a solid NP. Moreover, all these planar defects give rise to surface terraces, which may be of interest in relation to the increase of catalytic activity.[41]

In all the collision events we simulated, and before the transition from crater creation to perforation takes place, a partial surface recovery occurs, as can be seen in Figure 3. It is noticed that after a collision of a projectile with a velocity of 5.5 km/s 100% of the impacts are followed by self-repair; but, if the incident velocity is 6 km/s only 15% self-repairs. The same collision was simulated with the projectile impinging on a flat Pd film of the same thickness; however, no self-repair whatsoever did occur, an indication that it is related to intrinsic hNP properties, most likely related to surface stress due to the presence of the cavity.

A CNA analysis of the hNP after collision is shown in Figure 3a. It is noticed that a partial local shell amorphization occurs due to the impact and the subsequent local melting. During the first picoseconds, isolated bcc and hcp groups are formed, which give origin to stacking faults and twin boundaries as the structure starts to recrystallize. At the edges of the hNP coalesce, they and the damaged region partially self-heals. Figure 3b zooms into the damaged region, and the kinetic energy distribution is also illustrated, showing that a uniform distribution is reached upon recrystallization. In Figure 3c, the Von Misses stress is illustrated. Before the impact, an average stress of 12 MPa is present; however, since hNP are far from equilibrium, a residual stress due to the presence of the cavity is expected. This is similar to what has been reported for thin Pd films.[42] After the impact, the stress increase beyond 400 MPa on the impact region and both a plastic deformation and

DOI: 10.1021/acs.jpcc.7b03126
J. Phys. Chem. C 2017, 121, 17856−17861

perforation are observed. Finally, after 500 ps, the stress distribution becomes stable at 18 MPa.

Effects due to the thickness of the hNP on the amount of hcp defects are displayed in Figure 4. The hcp population always

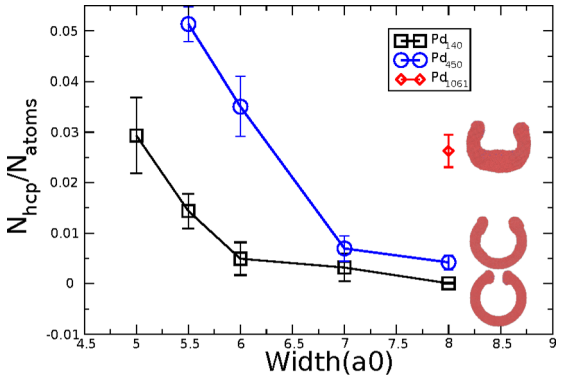

Figure 4. hNP hcp fraction after collision with Pd_{144}, Pd_{450}, and Pd_{1061} nanoclusters with a 10 km/s velocity, for several shell thicknesses. The illustrations on the right show the hNP cross section for $8a_0$ thickness. The single point for Pd_{1061} is included because of the bowl shape it creates; for thicknesses less than $8a_0$, the hNP collapses into a solid nanoparticle.

diminishes as the shell thickness increases; in fact, for thicknesses $>7a_0$, and for Pd_{144} and Pd_{450}, the defect presence is negligible. In all these collisions, the projectile energy is sufficient to perforate the hNP shell; however, it preserves its spherical shape and its crystal structure, as illustrated in the insets of the figure. On the other hand, when a Pd_{1061} collides with a $7a_0$ hNP, it is unable to withstand the impact and suffers a transition to a solid NP within a few picoseconds. This collapse is not related to thermal effects but simply to the large momentum that is transferred in the collision. For larger hNP thicknesses, a transition to a bowl-like shape takes place, as already reported by Zhong et al.,[43] who studied the transition of nanospheres to nanorings during reactive etching of SiO_2 NPs.

All of the above is limited to central ($b = 0$) collisions. However, the resulting damage on the hNP is strongly dependent on impact parameter b, as illustrated in Figure 5. The main reason for this dependence is that as b increases, part of the energy is released by sputtering, instead of contributing to raise the hNP temperature. Moreover, as can be seen in Figure 5b, there is a correlation between b and the generation of hcp, which reaches a minimum for $b/R = 0.5$. This minimum occurs at the intersection of two ⟨111⟩ planes, which originate hcp defects for $b/R \approx 0$ and $b/R \approx 1.0$, when four ⟨111⟩ intersect, increasing the probability of generating sliding planes and consequently the possibility of hcp finding regions.

The last issue we explored is the hNP resistance when subject to consecutive collisions, shown in Figure 6. Each collision impact point is different from the previous ones and occurs after the energy acquired by the hNP is dissipated. When the projectile impinges on a stacking fault or twin, a reduction of the hcp fraction is observed during the first few instants after the collision takes place, due to local melting and subsequent shell perforation. When after the first collisions shell perforations do occur, the hNP still retains its spherical shape. However, after approximately the sixth collision the hNP shrinks, losing its initial form, and adopts a truncated cuboctahedral highly faceted structure. Moreover, all hcp atoms illustrated in Figure 6 correspond to planar defects

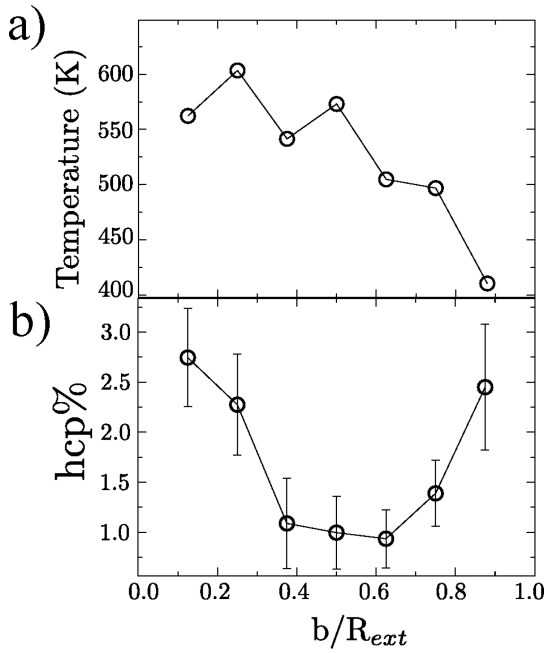

Figure 5. (a) and (b) show the temperature and fraction of hcp, respectively, as a function of impact parameter. The hNPs were impinged by Pd_{144} NPs with a 10 km/s speed.

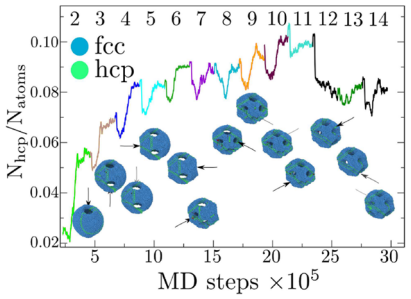

Figure 6. Evolution of the hNP after successive collisions. After each collision energy is dissipated, and the temperature set at 300 K. The atom coloring is hcp (green), fcc (blue), and bcc (red). Atoms with different coordination were removed from the figure. The arrows point to the place the projectile impacts. The numbers on top indicate the number of collisions the hNP has suffered.

such as stacking faults or twin boundaries. Since the hNP width is 2 nm, every planar defect leads to the formation of a surface step. Therefore, a hNP with a larger hcp population could present an important number of surface steps that can be used to increase catalytic activity. After 12 collisions, the N_{hcp}/N_{atoms} fraction remains stable at 0.08 and the hNP adopts a shape similar to the hollow nanoframes[44,45] or nanocages[46] that have been synthesized experimentally.

CONCLUSIONS

The interest in Pd for hydrogen storage and catalysis is long dated. Above, we explored the properties and the potential applications of hNP to improve their performance. To maximize the efficient use of Pd hNPs, a key issue is to gain access to the interior cavity. To do so, we investigated the feasibility of creating channels across their shells, to allow easy passage of molecules to the inner cavity. This way the surface available increases significantly.

DOI: 10.1021/acs.jpcc.7b03126
J. Phys. Chem. C 2017, 121, 17856−17861

We have shown that by bombardment with Pd NPs of adequate size and speed, it is feasible to open such channels. To achieve this objective the projectile has to be large enough for the channel to open and the collision not too violent so that the hNP integrity is preserved. While hNPs could be perceived as fragile and subject to collapse, we showed that there is a range of energy and wall thicknesses, and ratios of inner and outer radii values, that allows to bore the channels that are required. To achieve our goals we simulated, by means of classical molecular dynamics (MD), the collision of hypervelocity nanoprojectiles (between 3 a 15 km/s) and Pd hNPs. Nevertheless, several issues remain open for further study. We limited our attention to free-standing hNPs; however, the energy dissipation for supported targets may increase the allowed energy range. Other sizes, especially large ones, and other shell-to-diameter ratios may also be able to withstand collisions.

We start by showing that the hNP remains stable within a relatively large range of projectile energies. Next we simulate the dynamics for a variety of projectile sizes and obtain a lower limit for perforation of the shell and a maximum beyond which the hNP collapses after impact. The type of defects that are created in the Pd hNP is explored and shed some light on the energy transfer dynamics. Depending on the energy deposited on the hNP, craters or channels are created. Previously the creation of craters had only been reported as a result of synthesis.

We also simulated collisions for the whole range of impact parameters and studied what happens when the target is subject to successive collisions. In fact, the hNP is able to withstand a series of consecutive impacts. Moreover, after several projectiles impact the target, a transition from spherical to faceted is observed, giving origin to porous structures like nanoframes[44] or hollow truncated cube-octahedron nanoparticles with a large population of planar defects[46] but with a lower total potential energy than the original spherical hNP structure, due to the partial shrinkage. Since hNPs display a high catalytic performance, the formation of multiple channels, high facet index surfaces,[47,48] and surface steps could increase even further the catalytic activity in Pd-based nanostructures.

The Pd hNPs do collapse when: (i) the temperature increase due to the collision is large enough to generate a self-diffusion process, as found in the experiment;[23,24] (ii) the radius of the projectile is on the order of the size of the target; in that case the hNP is destroyed during the first picoseconds after impact.

All of our results suggest that hNPs are resilient under impact and therefore may be useful in many practical applications, in analogy to materials built with macroscopic hollow spheres.[19,20] In fact, these macroscopic structures are used to protect against impact, for example in airplane cockpits, since they are able to dissipate energy efficiently because of their large free volumes and surfaces which allow them to accommodate defects. At the same time, this suggests new possibilities: a material made of hNPs could present similar radiation-resistant properties as macroscopic metal nanofoams.[49−51] Moreover, since they are so resilient, they may withstand SHI impact, highly charged ions, or keV single ion irradiation.

AUTHOR INFORMATION

Corresponding Author

*E-mail: m.kiwi.t@gmail.com.

ORCID

Rafael I. González: 0000-0003-2599-8404

Miguel Kiwi: 0000-0001-8580-1912

Notes

The authors declare no competing financial interest.

ACKNOWLEDGMENTS

This work was supported by the Fondo Nacional de Investigaciones Científicas y Tecnológicas (FONDECYT, Chile) under Grants #1160639 and 1130272 (M.K. and J.R.), 1150718 (J.A.V.) AFOSR Grant FA9550-16-1-0122 (J.A.V. and M.K.), and Financiamiento Basal para Centros Científicos y Tecnológicos de Excelencia FB-0807 (R.G., F.V., J.M., M.K., and J.R.). E.M.B. thanks support from the PICT-2014-0696 (ANPCyT) and M003 (SeCTyP-UN Cuyo) Grants. F.V. was supported by CONICYT Doctoral Fellowship Grant 21140948.

REFERENCES

(1) Crespo, E. A.; Ruda, M.; de Debiaggi, S. R.; Bringa, E. M.; Braschi, F. U.; Bertolino, G. Hydrogen Absorption in Pd Nanoparticles of Different Shapes. *Int. J. Hydrogen Energy* **2012**, *37*, 14831−14837.

(2) Crespo, E.; Claramonte, S.; Ruda, M.; de Debiaggi, S. R. Thermodynamics of Hydrogen in Pd Nanoparticles. *Int. J. Hydrogen Energy* **2010**, *35*, 6037−6041.

(3) Ruda, M.; Crespo, E.; de Debiaggi, S. R. Atomistic Modeling of H Absorption in Pd Nanoparticles. *J. Alloys Compd.* **2010**, *495*, 471−475.

(4) Kim, S.-W.; Kim, M.; Lee, W. Y.; Hyeon, T. Fabrication of Hollow Palladium Spheres and their Successful Application to the Recyclable Heterogeneous Catalyst for Suzuki Coupling Reactions. *J. Am. Chem. Soc.* **2002**, *124*, 7642−7643.

(5) Koo, B.; Xiong, H.; Slater, M. D.; Prakapenka, V. B.; Balasubramanian, M.; Podsiadlo, P.; Johnson, C. S.; Rajh, T.; Shevchenko, E. V. Hollow Iron Oxide Nanoparticles for Application in Lithium Ion Batteries. *Nano Lett.* **2012**, *12*, 2429−2435.

(6) Wang, B.; Chen, J. S.; Wu, H. B.; Wang, Z.; Lou, X. W. Quasiemulsion-Templated Formation of α-Fe_2O_3 Hollow Spheres with Enhanced Lithium Storage Properties. *J. Am. Chem. Soc.* **2011**, *133*, 17146−17148.

(7) Chen, J. S.; Luan, D.; Li, C. M.; Boey, F. Y. C.; Qiao, S.; Lou, X. W. TiO_2 and SnO_2@ TiO_2 Hollow Spheres Assembled from Anatase TiO_2 Nanosheets with Enhanced Lithium Storage Properties. *Chem. Commun.* **2009**, *46*, 8252−8254.

(8) Ge, J.; Xing, W.; Xue, X.; Liu, C.; Lu, T.; Liao, J. Controllable Synthesis of Pd Nanocatalysts for Direct Formic Acid Fuel Cell (DFAFC) Application: from Pd Hollow Nanospheres to Pd Nanoparticles. *J. Phys. Chem. C* **2007**, *111*, 17305−17310.

(9) Liu, Z.; Zhao, B.; Guo, C.; Sun, Y.; Shi, Y.; Yang, H.; Li, Z. Carbon Nanotube/Raspberry Hollow Pd Nanosphere Hybrids for Methanol, Ethanol, and Formic Acid Electro-Oxidation in Alkaline Media. *J. Colloid Interface Sci.* **2010**, *351*, 233−238.

(10) Wang, B.; Yang, J.; Wang, L.; Wang, R.; Tian, C.; Jiang, B.; Tian, M.; Fu, H. Hollow Palladium Nanospheres with Porous Shells Supported on Graphene as Enhanced Electrocatalysts for Formic Acid Oxidation. *Phys. Chem. Chem. Phys.* **2013**, *15*, 19353−19359.

(11) Chen, D.; Cui, P.; He, H.; Liu, H.; Yang, J. Highly Catalytic Hollow Palladium Nanoparticles Derived from Silver@Silver-Palladium CoreShell Nanostructures for the Oxidation of Formic Acid. *J. Power Sources* **2014**, *272*, 152−159.

(12) Tang, S.; Vongehr, S.; Wang, X.; Wang, Y.; Meng, X. Bubble-Assisted Growth of Hollow Palladium Nanospheres with Structure Control Allowing Very Thin Shells for Highly Enhanced Catalysis. *RSC Adv.* **2014**, *4*, 13729−13732.

(13) Valencia, F. J.; González, R. I.; Tramontina, D.; Rogan, J.; Valdivia, J. A.; Kiwi, M.; Bringa, E. M. Hydrogen Storage in Palladium Hollow Nanoparticles. *J. Phys. Chem. C* **2016**, *120*, 23836−23841, DOI: 10.1021/acs.jpcc.6b07895.

(14) Mezzavilla, S.; Baldizzone, C.; Mayrhofer, K. J.; Schüth, F. General Method for the Synthesis of Hollow Mesoporous Carbon Spheres with Tunable Textural Properties. *ACS Appl. Mater. Interfaces* **2015**, *7*, 12914−12922.
(15) Jayaprakash, N.; Shen, J.; Moganty, S. S.; Corona, A.; Archer, L. A. Porous Hollow Carbon@ Sulfur Composites for High-Power Lithium-Sulfur Batteries. *Angew. Chem.* **2011**, *123*, 6026−6030.
(16) Chen, D.; Ye, J. Hierarchical WO_3 Hollow Shells: Dendrite, Sphere, Dumbbell, and their Photocatalytic Properties. *Adv. Funct. Mater.* **2008**, *18*, 1922−1928.
(17) Chen, H. M.; Liu, R.-S.; Lo, M.-Y.; Chang, S.-C.; Tsai, L.-D.; Peng, Y.-M.; Lee, J.-F. Hollow Platinum Spheres with Nano-Channels: Synthesis and Enhanced Catalysis for Oxygen Reduction. *J. Phys. Chem. C* **2008**, *112*, 7522−7526.
(18) Wang, L.; Yamauchi, Y. Metallic Nanocages: Synthesis of Bimetallic Pt-Pd Hollow Nanoparticles with Dendritic Shells by Selective Chemical Etching. *J. Am. Chem. Soc.* **2013**, *135*, 16762−16765.
(19) Li, Z.-Z.; Wen, L.-X.; Shao, L.; Chen, J.-F. Fabrication of Porous Hollow Silica Nanoparticles and their Applications in Drug Release Control. *J. Controlled Release* **2004**, *98*, 245−254.
(20) Zeng, H.; Pattofatto, S.; Zhao, H.; Girard, Y.; Fascio, V. Perforation of Sandwich Plates with Graded Hollow Sphere Cores Under Impact Loading. *Int. J. Impact Eng.* **2010**, *37*, 1083−1091.
(21) Jiang, L.; Yin, X.; Zhao, J.; Liu, H.; Liu, Y.; Wang, F.; Zhu, J.; Boey, F.; Zhang, H. Theoretical Investigation on the Thermal Stability of Hollow Gold Nanoparticles. *J. Phys. Chem. C* **2009**, *113*, 20193−20197.
(22) Jiang, L.; Sun, W.; Gao, Y.; Zhao, J. Geometric Thermal Phase Diagrams for Studying the Thermal Dynamic Stability of Hollow Gold Nanoballs at Different Temperatures. *Phys. Chem. Chem. Phys.* **2014**, *16*, 6623−6629.
(23) Nakamura, R.; Tokozakura, D.; Lee, J.-G.; Mori, H.; Nakajima, H. Shrinking of Hollow Cu_2O and NiO Nanoparticles at High Temperatures. *Acta Mater.* **2008**, *56*, 5276−5284.
(24) Glodán, G.; Cserháti, C.; Beke, D. L. Temperature-Dependent Formation and Shrinkage of Hollow Shells in Hemispherical Ag/Pd Nanoparticles. *Philos. Mag.* **2012**, *92*, 3806−3812.
(25) Huang, R.; Shao, G.-F.; Zeng, X.-M.; Wen, Y.-H. Diverse Melting Modes and Structural Collapse of Hollow Bimetallic Core-Shell Nanoparticles: A Perspective from Molecular Dynamics Simulations. *Sci. Rep.* **2015**, *4*, 2045.
(26) Shan, Z.; Adesso, G.; Cabot, A.; Sherburne, M.; Syed Asif, S. A.; Warren, O.; Chrzan, D.; Minor, A.; Alivisatos, A. Ultrahigh Stress and Strain in Hierarchically Structured Hollow Nanoparticles. *Nat. Mater.* **2008**, *7*, 947−952.
(27) Yang, L.; Bian, J.; Zhang, H.; Niu, X.; Wang, G. Size-Dependent Deformation Mechanisms in Hollow Silicon Nanoparticles. *AIP Adv.* **2015**, *5*, 077162.
(28) Plimpton, S. Fast Parallel Algorithms for Short-Range Molecular Dynamics. *J. Comput. Phys.* **1995**, *117*, 1−19.
(29) Daw, M. S.; Baskes, M. I. Embedded-atom method: Derivation and Application to Impurities, Surfaces, and Other Defects in Metals. *Phys. Rev. B: Condens. Matter Mater. Phys.* **1984**, *29*, 6443.
(30) Sheng, H.; Kramer, M.; Cadien, A.; Fujita, T.; Chen, M. Highly Optimized Embedded-Atom-Method Potentials for Fourteen fcc Metals. *Phys. Rev. B: Condens. Matter Mater. Phys.* **2011**, *83*, 134118.
(31) Paradis, P. F.; Ishikawa, T.; Saita, Y.; Yoda, S. Containerless Property Measurements of Liquid Palladium. *Int. J. Thermophys.* **2004**, *25*, 1905−1912.
(32) Mao, H.; Bell, P.; Shaner, J. t.; Steinberg, D. Specific Volume Measurements of Cu, Mo, Pd, and Ag and Calibration of the Ruby R1 Fluorescence Pressure Gauge from 0.06 to 1 Mbar. *J. Appl. Phys.* **1978**, *49*, 3276−3283.
(33) Shan, A.; Chen, Z.; Li, B.; Chen, C.; Wang, R. Monodispersed, Ultrathin NiPt Hollow Nanospheres with Tunable Diameter and Composition Via a Green Chemical Synthesis. *J. Mater. Chem. A* **2015**, *3*, 1031−1036.
(34) Ziegler, J. *Stopping and Ranges in Matter (SRIM)*, 2009.
(35) Stukowski, A. Visualization and Analysis of Atomistic Simulation Data with OVITOthe Open Visualization Tool. *Modell. Simul. Mater. Sci. Eng.* **2010**, *18*, 015012.
(36) Gupta, S. K.; Talati, M.; Jha, P. K. Shape and Size Dependent Melting Point Temperature of Nanoparticles. Mat. *Mater. Sci. Forum* **2008**, *570*, 132−137.
(37) Cour-Palais, B. G. Space Vehicle Meteoroid Shielding Design. *Comet Halley Micrometeoroid Hazard Workshop: Proceedings of an International Workshop held in ESTEC*, Noordwijk, The Netherlands, April 18−19, 1979; The Agency: Ann Arbor, Michigan, 1979.
(38) Higginbotham, A.; Bringa, E.; Taylor, E. A.; Graham, G. Penetration Scaling in Atomistic Simulations of Hypervelocity Impact. *Int. J. Impact Eng.* **2011**, *38*, 247−251.
(39) Millán, E. N.; Tramontina, D. R.; Urbassek, H. M.; Bringa, E. M. Nucleation of Plasticity in Nanoparticle Collisions. *Phys. Rev. E: Stat. Phys., Plasmas, Fluids, Relat. Interdiscip. Top.* **2016**, *93*, 063004.
(40) Millán, E. N.; Tramontina, D. R.; Urbassek, H. M.; Bringa, E. M. The Elastic-Plastic Transition in Nanoparticle Collisions. *Phys. Chem. Chem. Phys.* **2016**, *18*, 3423−3429.
(41) Dahl, S.; Logadottir, A.; Egeberg, R.; Larsen, J.; Chorkendorff, I.; Törnqvist, E.; Nørskov, J. K. Role of Steps in N_2 Activation on Ru (0001). *Phys. Rev. Lett.* **1999**, *83*, 1814.
(42) Ramos De Debiaggi, S.; Crespo, E.; Braschi, F.; Bringa, E.; Alí, M.; Ruda, M. Hydrogen Absorption in Pd Thin-films. *Int. J. Hydrogen Energy* **2014**, *39*, 8590−8595.
(43) Zhong, K.; Li, J.; Liu, L.; Brullot, W.; Bloemen, M.; Volodin, A.; Song, K.; Van Dorpe, P.; Verellen, N.; Clays, K. Direct Fabrication of Monodisperse Silica Nanorings from Hollow Spheres−A Template for Core−Shell Nanorings. *ACS Appl. Mater. Interfaces* **2016**, *8*, 10451−10458.
(44) Kim, D.; Park, J.; An, K.; Yang, N.-K.; Park, J.-G.; Hyeon, T. Synthesis of Hollow Iron Nanoframes. *J. Am. Chem. Soc.* **2007**, *129*, 5812−5813.
(45) Lu, X.; Au, L.; McLellan, J.; Li, Z.-Y.; Marquez, M.; Xia, Y. Fabrication of Cubic Nanocages and Nanoframes by Dealloying Au/Ag Alloy Nanoboxes with an Aqueous Etchant Based on Fe $(NO)_3$ or NH_4OH. *Nano Lett.* **2007**, *7*, 1764−1769.
(46) Cobley, C. M.; Xia, Y. Engineering the Properties of Metal Nanostructures Via Galvanic Replacement Reactions. *Mater. Sci. Eng., R* **2010**, *70*, 44−62.
(47) Su, N.; Chen, X.; Yue, B.; He, H. Formation of Palladium Concave Nanocrystals Via Auto-catalytic Tip Overgrowth by Interplay of Reduction Kinetics, Concentration Gradient and Surface Diffusion. *Nanoscale* **2016**, *8*, 8673−8680.
(48) Yu, S.; Zhang, L.; Zhao, Z.-J.; Gong, J. Structural Evolution of Concave Trimetallic Nanocubes with Tunable Ultra-thin Shells for Oxygen Reduction Reaction. *Nanoscale* **2016**, *8*, 16640−16649.
(49) Anders, C.; Bringa, E. M.; Urbassek, H. M. Sputtering of a metal nanofoam by Au ions. *Nucl. Instrum. Methods Phys. Res., Sect. B* **2015**, *342*, 234−239.
(50) Bringa, E.; Monk, J.; Caro, A.; Misra, A.; Zepeda-Ruiz, L.; Duchaineau, M.; Abraham, F.; Nastasi, M.; Picraux, S.; Wang, Y.; et al. Are Nanoporous Materials Radiation Resistant? *Nano Lett.* **2012**, *12*, 3351−3355.
(51) Beyerlein, I.; Caro, A.; Demkowicz, M.; Mara, N.; Misra, A.; Uberuaga, B. Radiation Damage Tolerant Nanomaterials. *Mater. Today* **2013**, *16*, 443−449.

DOI: 10.1021/acs.jpcc.7b03126
J. Phys. Chem. C 2017, 121, 17856−17861